ELSEVIER

Colloids and Surfaces
A: Physicochemical and Engineering Aspects 176 (2001) 69–83

COLLOIDS AND SURFACES A

www.elsevier.nl/locate/colsurfa

Alkyl polyglucoside microemulsion phase behavior

Larry D. Ryan [1], Eric W. Kaler *

Department of Chemical Engineering, Center for Molecular and Engineering Thermodynamics, University of Delaware, Newark, DE 19716, USA

Received 25 January 1999; accepted 17 April 2000

Abstract

We review several key elements of alkyl polyglucoside (C_mG_n) microemulsion phase behavior. The low solubility of C_mG_n surfactants in oils such as alkanes makes producing C_mG_n microemulsions and subsequent study of their phase behavior difficult. Increasing the solubility of C_mG_n in oil is therefore helpful for the systematic study of C_mG_n-based microemulsion formulations. To this end, the role of cosurfactants in producing microemulsions with water, alkanes, and n-alkyl β-D-glucopyranosides is first discussed. Adding $C_{10}\beta G_1$ to mixtures of water–alkane–ethoxylated alcohol surfactants (C_iE_j) produces a region of the three-phase body (a 'chimney') that is independent of temperature; thus $C_m\beta G_1$ are not completely soluble in the co-oil formed of alkane and C_iE_j at higher temperatures. Then, through a novel approach using oxygenated ether oils ($C_kOC_2OC_k$), microemulsions are formed with water, $C_kOC_2OC_k$, and $C_m\beta G_1$ and the phase behavior studied as a function of temperature and composition. Increased $C_m\beta G_1$ solubility in the more hydrophilic ether oils produces patterns of phase behavior in water–$C_kOC_2OC_k$–$C_m\beta G_1$ mixtures that are identical to those observed in water–alkane–C_iE_j mixtures. Using the water–ether oil–$C_m\beta G_1$ mixtures as a base case, the role of C_mG_n surfactant structure in setting C_mG_n microemulsion phase behavior is explored. The solubility of the α-D anomer (n-alkyl α-D-glucopyranosides, $C_m\alpha G_1$) in water is much less than that of the β-D surfactant, and these solubility boundaries extend to high surfactant and oil concentrations in water–$C_kOC_2OC_k$–$C_m\alpha G_1$ mixtures. Adding C_mG_2 compounds to water–$C_kOC_2OC_k$–$C_m\beta G_1$ mixtures shifts the phase behavior to high temperatures, again demonstrating the extreme hydrophilic nature of the sugar headgroup. Finally, adding small amounts of ionic alkyl sulfate surfactants to water–$C_kOC_2OC_k$–$C_m\beta G_1$ mixtures dramatically reduces the total amount of surfactant needed to form a single-phase microemulsion.

Keywords: Alkyl polyglucoside; Water; Oil

1. Introduction

Alkyl polyglucosides (C_mG_n, where m is the number of carbon atoms in the alkyl chain and n the number of glucose units in the hydrophilic head group) are an interesting class of nonionic surfactants that have received considerable re-

* Corresponding author.
[1] Present address: GE Silicones, 260 Hudson River Rd., Bldg. 14/35, Waterford, NY 12188, USA.

0927-7757/01/$ - see front matter
PII: S0927-7757(00)00614-2

search attention in recent years [1–6]. These surfactants are particularly desirable as a result of excellent biodegradability and ease of manufacture from renewable resources such as sugar and vegetable oil feedstocks [7]. However, although the popularity of this class of materials has increased substantially, relatively little is known about the physical and chemical characteristics of C_mG_n surfactants in solution. Increased understanding of the fundamental properties of C_mG_n surfactants would lead to better utilization in several industrial applications.

One potential use for C_mG_n surfactants is in microemulsion formulations. Microemulsions are thermodynamically stable, isotropic mixtures containing water, oil, and surfactant (and possibly other additives such as salt or alcohol), and are utilized in a variety of industrial applications (e.g. enhanced oil recovery, solvent delivery, and polymerization) [3,8]. Producing microemulsions with water, alkanes, and nonionic surfactants (C_iE_j, which contain *i* number of carbon atoms in the alkyl chain and *j* ethoxy units in the head group) is a well established practice, and much time and effort has been spent recording the patterns of phase behavior observed in water–alkane–C_iE_j mixtures [9–14]. These mixtures provide an excellent basis for comparison with other water–oil–nonionic surfactant mixtures.

The omnipresent characteristic of water–alkane–C_iE_j phase behavior is the change in the partitioning of the surfactant from the water-rich to oil-rich phase with increasing temperature, resulting in the well known $\underline{2}$–3–$\overline{2}$ or $\underline{2}$–1–$\overline{2}$ phase sequence, depending on the total surfactant concentration. In this notation the bar denotes the phase in which the surfactant is mainly dissolved. Study of water–alkane–C_iE_j mixtures shows that the most important properties involved in determining the temperature range of the three-phase body (and hence the $\underline{2}$–3–$\overline{2}$ phase sequence) are (1) the temperature associated with the critical endpoint (cep_β) of the critical line extending from the critical point (cp_β at T_β) in the water–C_iE_j mixture; and (2) the temperature associated with the critical endpoint (cep_α) of the critical line extending from the critical point (cp_α at T_α) in the alkane–C_iE_j binary mixture. Therefore, knowledge of T_α and T_β is crucial for choosing surfactants and making microemulsions within a specified temperature range. Extreme values of T_α or T_β (or both) can make producing a microemulsion at desired conditions impossible for a given water–oil–nonionic surfactant mixture.

Making microemulsions with C_mG_n is difficult as a result of low surfactant solubility in many classes of oils, most notably normal alkanes. Therefore, T_α is extremely high, requiring the use of a cosurfactant to enhance C_mG_n oil solubility and produce microemulsions in water–alkane–C_mG_n mixtures. Several groups [15–21] (including some of the work described here [22]) have explored this approach and studied the phase behavior and properties of water–alkane–C_mG_n–cosurfactant microemulsions. However, although cosurfactants are quite useful in practical situations, they can mask some of the properties of the surfactant in setting the phase behavior.

Fundamentally, it is of substantial interest to form C_mG_n-based microemulsions without the use of a cosurfactant so the intrinsic behavior of these surfactants may be established. We chose oxygenated 'ether oils' ($C_kOC_2OC_k$, where *k* is the length of the alkyl ether chains) as suitable candidates for C_mG_n microemulsion formulation. C_mG_n are soluble in $C_kOC_2OC_k$ at higher temperatures and T_α is located within the experimental window (0–80°C). As will be discussed below [23], lowering the value of T_α allows water–$C_kOC_2OC_k$–C_mG_n mixtures to produce patterns of phase behavior identical to that observed in other nonionic surfactant microemulsion mixtures.

The establishment of novel water–$C_kOC_2OC_k$–$C_m\beta G_1$ microemulsions allows probing of the effect of several experimental variables (i.e. surfactant structure and ionic surfactant additives) on the phase behavior. Aside from variation of *m* or *n*, C_mG_n possess an additional structural degree of freedom as a result of the anomeric orientation of the sugar headgroup into the α-D ($C_m\alpha G_1$) or β-D ($C_m\beta G_1$) form. The α-D anomer has a more stable crystalline structure than the β-D anomer [24–28], and this increased crystalline stability has large ramifications on the stability of

water–$C_kOC_2OC_k$–$C_m\alpha G_1$ microemulsions [29]. The use of ionic surfactants as additives in water–alkane–C_iE_j mixtures produces increased microemulsion stability and requires substantially lower amounts of surfactant to microemulsify equal amounts of oil and water [30]. Similarly, adding alkyl sulfates to water–$C_kOC_2OC_k$–$C_m\beta G_1$ mixtures produces large changes in the phase behavior [31], and below we briefly discuss the mechanisms responsible for these observed effects.

In this paper we review several aspects of C_mG_n-based microemulsion phase behavior. First, the phase behavior of water–octane–C_6E_2–$C_{10}\beta G_1$ mixtures is explored as a function of increasing $C_{10}\beta G_1$ concentration, demonstrating the role of cosurfactants in forming microemulsions with C_mG_n and alkanes. Then, through the use of ether oils, novel water–$C_kOC_2OC_k$–$C_m\beta G_1$ microemulsions are formed and their phase studied as a function of temperature and surfactant concentration. Substituting the α-D for β-D form allows the study of the effect of the anomeric nature of the sugar headgroup on the phase behavior of water–$C_kOC_2OC_k$–C_mG_1 mixtures. Adding C_mG_2 compounds to water–$C_kOC_2OC_k$–$C_m\beta G_1$ mixtures shows how increasing the hydrophilicity of the surfactant effects the temperature range of the three-phase body and single-phase microemulsion region. Finally, minute amounts of alkyl sulfate are added to water–$C_kOC_2OC_k$–$C_m\beta G_1$ mixtures and the changes in phase behavior recorded as a function of temperature and composition.

2. Phase diagram determination

The methodology used to study C_mG_n microemulsion phase behavior follows that introduced by Kahlweit and coworkers [13,32] for a quaternary mixture of water (A)–oil (B)–surfactant 1 (C)–surfactant 2 (D). In a four component mixture five independent variables; pressure (P), temperature (T), and three mass fractions unambiguously define the phase space. The following composition variables are most suitable for our purposes and are defined as the mass ratio of oil to water plus water in the mixture, α:

$$\alpha = \frac{A}{A+B} \times 100 \quad \text{in} \quad \text{wt\%}, \tag{1}$$

the mass fraction of surfactant in the mixture, γ:

$$\gamma = \frac{C+D}{A+B+C+D} \times 100 \quad \text{in} \quad \text{wt\%}, \tag{2}$$

and when two surfactants are used the mass fraction of surfactant D in the mixture, δ:

$$\delta = \frac{D}{C+D} \times 100 \quad \text{in} \quad \text{wt\%}. \tag{3}$$

Making a two-dimensional phase diagram for a quaternary mixture (with pressure constant at ambient) requires that two of the remaining variables T, α, γ, and δ be held constant.

One section through the phase prism that has shown to be especially useful when studying microemulsion phase behavior is a section containing equal masses of oil and water ($\alpha = 50$) probed as a function of temperature and surfactant concentration. This section allows the determination of the least amount of surfactant necessary to completely solubilize equal masses of oil and water [or the efficiency, denoted by ($\tilde{\gamma}$)] and the extent and average temperature ($\tilde{T}$) of the three-phase body for a given oil [33].

The procedure used to determine the phase boundaries for sections through the phase prism for the water–oil–C_mG_n–cosurfactant mixtures closely follows that of Schubert and Strey [34]. For the sections through the phase prism as a function of temperature the phase boundaries were determined to within 0.05°C, while the phase boundaries of sections at constant temperature were determined to within 1 wt%.

3. Phase behavior results and discussion

3.1. Water–$C_m\beta G_1$ and alkane–$C_m\beta G_1$ mixtures

Fig. 1 shows the temperature-composition phase diagrams of binary water–C_mG_1 mixtures for $m = 10$ and 12. Both surfactants have a large miscibility gap at low surfactant concentrations. For water–$C_{10}\beta G_1$ a Krafft boundary occurs at 22.5°C, while for water–$C_{12}\beta G_1$ it appears at 37.5°C. Solutions below the Krafft boundary are

metastable, and the dashed lines in Fig. 1 show the limits of this metastable region before crystal formation in the water–$C_{10}\beta G_1$ mixture. The miscibility gap in the water–$C_{12}\beta G_1$ mixture extends over a larger concentration range than that in the water–$C_{10}\beta G_1$ mixture, which is one indication that T_β is much lower for $C_{12}\beta G_1$. The actual value of T_β for either $C_{10}\beta G_1$ or $C_{12}\beta G_1$ is obscured by the Krafft boundary. The solid and open squares show the reported critical micelle concentration (cmc) for $C_{10}\beta G_1$ and $C_{12}\beta G_1$, respectively [6,35]. When $m < 10$, $C_m\beta G_1$ are completely miscible with water throughout the experimental temperature range, demonstrating that T_β rises sharply with decreasing alkyl chain length.

3.2. Role of cosurfactants

The use of cosurfactants is a well established practice for either shifting existing microemulsion phase behavior to different experimental conditions or producing microemulsions in mixtures that otherwise exhibit stable emulsions over a large range of temperature and composition. C_iE_j surfactants were chosen especially as cosurfactants for C_mG_n microemulsions because the phase behavior of water–alkane–C_iE_j mixtures is well

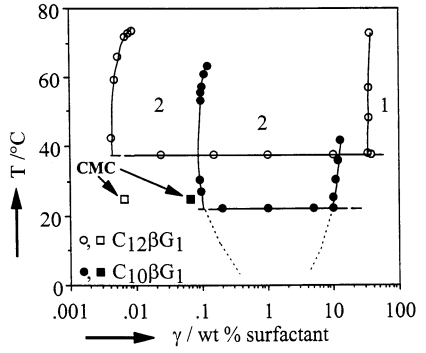

Fig. 1. Binary phase diagrams for water–$C_m\beta G_1$ mixtures as a function of temperature and composition for $m = 10$ and 12. The lightly dashed lines (- - - -) mark the boundaries of a metastable two-phase region present in the water–$C_{10}\beta G_1$ mixture. The squares shows the critical micelle concentrations reported by Shinoda [35] for the water–$C_{10}\beta G_1$ and water–$C_{12}\beta G_1$ mixtures. The solid, horizontal lines mark the presence of a Krafft boundary.

understood, and therefore perturbing these mixtures with $C_m\beta G_1$ allows for the direct determination of some $C_m\beta G_1$ properties in solution.

3.2.1. Phase behavior for water (A) –octane (B) –C_6E_2 (C) –$C_{10}\beta G_1$ (D)

Fig. 2 shows the temperature-composition phase diagram for the water–octane–C_6E_2–$C_{10}\beta G_1$ mixture for $\delta = 10$ (top), 25 (center) and 50 (bottom) at $\alpha = 50$. The water–octane–C_6E_2 'fish' ($\delta = 0$) is shown for reference in each plot. Adding $C_{10}\beta G_1$ cause the homogeneous microemulsion region ('fish tail') to widen and slightly increases the efficiency of the surfactant mixture (i.e. $\tilde{\gamma} = 33$ for $\delta = 0$ and drops to $\tilde{\gamma} = 31$ for $\delta = 10$). The temperature interval of the three-phase body increases with increasing δ, and the whole three-phase region moves up in temperature. The dominating feature of these phase diagrams is the emergence of a region in the three-phase body that is almost independent of temperature (a so-called 'chimney') which begins at γ^* (shown by the dashed line in Fig. 2 (top)) as γ is decreased in the presence of $C_{10}\beta G_1$. The concentration range of the 'chimney' region is a function of δ. For example, at $\delta = 10$, the 'chimney' region emerges at $\gamma^* = 7$ and extends to $\gamma = 2$, while at $\delta = 50$ the 'chimney' region begins at $\gamma^* = 25$ and still extends to $\gamma = 3$, making the entire 'fish body' almost independent of temperature. At very low δ ($\delta = 1$) the 'chimney' is extremely narrow and very difficult to observe experimentally.

3.2.2. Section through phase tetrahedron at $\alpha = 50$, varying γ and δ

Fig. 3 (top) shows a schematic of a section through the water–octane–C_6E_2–$C_{10}\beta G_1$ phase tetrahedron at $\alpha = 50$ as a function of δ and γ. Experimental data [Fig. 3 (bottom)] is shown for this mixture at 25 and 60°C. At 25°C, C_6E_2 is mainly dissolved in the oil ($\bar{2}$), so the two-phase region at low δ is also $\bar{2}$. As δ is increased, the three-phase body is traversed. At higher values of δ there is another two-phase region, $\underline{2}$, because $C_{10}\beta G_1$ is mainly dissolved in the water ($\underline{2}$) at 25°C. At high values of δ, stable emulsions form. The three-phase body starts at very low values of

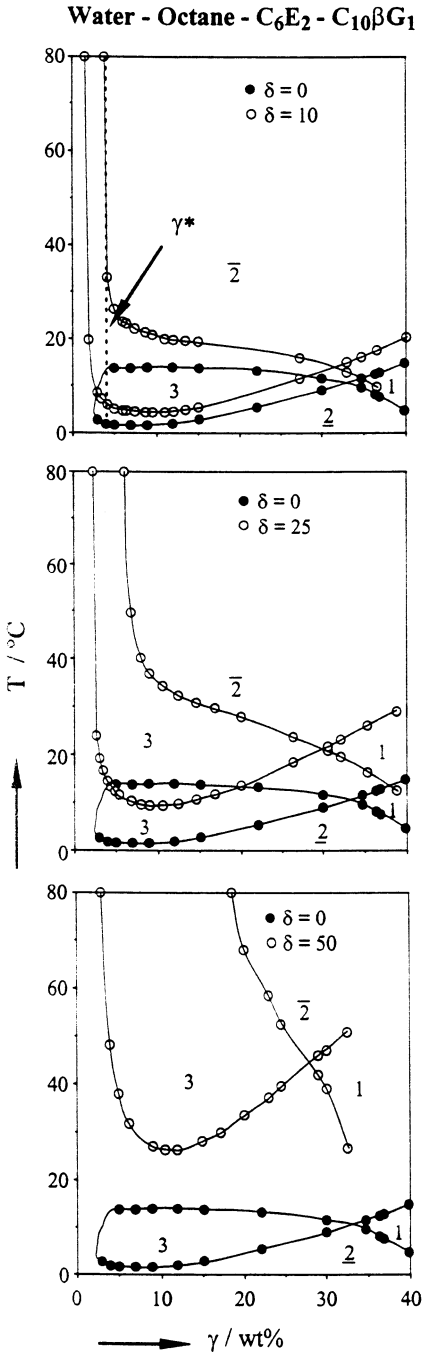

Fig. 2. Vertical sections through the pseudoternary phase prism for water–octane–C_6E_2–$C_{10}\beta G_1$ with varying $C_{10}\beta G_1$ concentration (δ) at equal mass fractions of water and octane ($\alpha = 50$) for $\delta = 10$ (top), $\delta = 25$ (center), and $\delta = 50$ (bottom).

δ ($\delta < 1$) and at low values of γ ($2 < \gamma < 5$). As γ increases, the amount of $C_{10}\beta G_1$ needed to promote the three-phase region also increases. The three-phase body extends to a maximum δ ($\delta = 48$) at $\gamma = 12$. The minimum amount of total surfactant necessary to form a one-phase microemulsion is $\gamma = 28.6$.

At 60°C, C_6E_2 remains dissolved in the oil and the same $\underline{2}$–3–$\overline{2}$ phase sequence is observed with increasing δ. However, the three-phase body shifts to higher δ, indicating an increased presence of $C_{10}\beta G_1$ in the microemulsion. The three-phase body extends to a maximum δ ($\delta = 68$) at $\gamma = 13$. At low values of δ and γ, the data for 25 and 60°C overlap, showing that the phase behavior in this region is essentially independent of temperature. Also, the minimum amount of surfactant needed to form the one-phase microemulsion remains constant at $\gamma = 28.6$, regardless of the increasing fraction of $C_{10}\beta G_1$.

The low γ and δ region of the diagram is of particular interest because the 'chimney' originates there. The three-phase body is present at very low δ ($\delta < 1$), showing that a small amount of $C_{10}\beta G_1$ in the mixture has substantial effects on

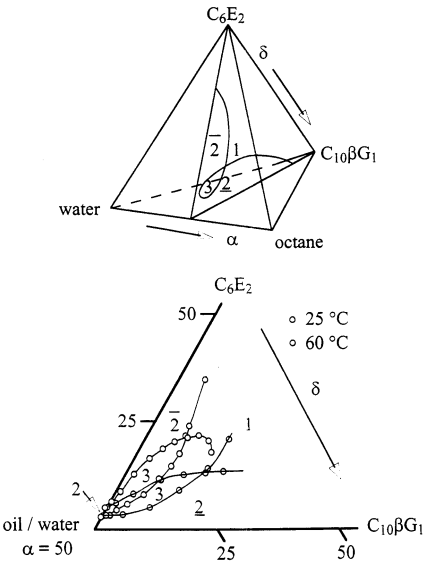

Fig. 3. A plane constructed in the constant temperature phase tetrahedron at $\alpha = 50$, with varying γ and δ with schematic (top) and experimental data for water–octane–C_6E_2–$C_{10}\beta G_1$ mixture at 25 and 60°C.

the phase behavior. Furthermore, the phase behavior in this region is essentially independent of temperature at a fixed δ, as supported by these results and observations shown in Fig. 1.

3.2.3. Cosurfactant discussion

The most pronounced feature of water–octane–C_iE_j–$C_m\beta G_1$ phase behavior is the formation of a temperature-independent region ('chimney') of the three-phase body at low surfactant concentration. The 'chimney' is observed regardless of the C_iE_j or $C_m\beta G_1$ examined. With increasing C_iE_j amphiphilicity (increasing *i* and *j*) the 'chimney' narrows, as does the entire three-phase region. Increasing $C_m\beta G_1$ alkyl chain length (and therefore the hydrophobicity) causes the 'chimney' to shrink. Furthermore, observation of water–octane–C_6E_2–$C_{10}\beta G_1$ samples at a fixed γ as a function of α and temperature shows that a large portion of the phase space contains a three-phase region that has nearly temperature-independent phase boundaries [22]. All of these phase behavior results illustrate that adding $C_m\beta G_1$ to water–alkane–C_iE_j mixtures interrupts the normal $\underline{2}$–3–$\overline{2}$ phase sequence always observed with increasing temperature. It is this failure to reach $\overline{2}$ in the 'chimney' that demonstrates the difficulty of forming microemulsions with $C_m\beta G_1$ and provides the unique feature of this phase behavior.

The characteristics of the binary water–$C_m\beta G_1$ and alkane–$C_m\beta G_1$ mixtures are large factors in determining $C_m\beta G_1$ microemulsion phase behavior. In water–$C_m\beta G_1$ mixtures for $m = 10$, T_β is located below 0°C, while for $m = 8$, T_β rises to more than 80°C [18]. For octane–$C_m\beta G_1$ mixtures, regardless of the value of *m*, $C_m\beta G_1$ are essentially insoluble in octane and T_α is above 80°C [18]. Although the value of T_β changes substantially with changes in *m*, the phase behavior of the water–octane–C_6E_2–$C_m\beta G_1$ mixtures remains qualitatively similar as *m* is varied; therefore the value of T_β plays a minor role in setting the phase behavior of these mixtures. Conversely, $C_m\beta G_1$ remain insoluble in octane regardless of the value of *m* and T_α is universally high. This property, coupled with the similarities in the quaternary phase behavior for water–octane–C_iE_j–$C_m\beta G_1$ mixtures for various *m* values, show that T_α and $C_m\beta G_1$ oil solubility are the dominating influences on the phase behavior.

The complex phase behavior resulting from the addition of $C_m\beta G_1$ to water–octane–C_iE_j mixtures is best understood when compared to the known phase behavior of quaternary mixtures of water, octane and two C_iE_j surfactants (C_iE_j and $C_iE_j^*$) [36,37]. Here the * merely denotes a different C_iE_j. Although there are similarities between the phase behavior of water–octane–C_iE_j–$C_iE_j^*$ mixtures and water–octane–C_iE_j–$C_m\beta G_1$ mixtures, the underlying phase behavior mechanisms are different. For a typical water–octane–C_iE_j–$C_iE_j^*$ mixture (e.g. water–octane–C_6E_2–$C_{12}E_8$ [22,36,37]), both surfactants are miscible in octane, T_α is low, and the phase behavior depends largely on the value of T_β for each of the water–surfactant pairs. Furthermore, T_α and T_β can not be independently adjusted, because increasing *i* or *j* will simultaneously decrease or increase the values of T_β and T_α. At high temperatures the upper critical tie-line is passed and both surfactants partition into the oil, producing a $\overline{2}$ region. For quaternary water–octane–C_iE_j–$C_m\beta G_1$ mixtures, the large changes in the value of T_β with changes in *m* have very little effect on the phase behavior. Also, $C_m\beta G_1$ are essentially insoluble in octane and T_α is located at high temperatures. Therefore, the phase behavior is dominated by the location of T_α and $C_m\beta G_1$ oil solubility. The C_iE_j act to increase the hydrophilicity of the octane, ultimately forming an octane–C_iE_j 'co-oil' in which the $C_m\beta G_1$ is more soluble than it is in alkane. However, although $C_m\beta G_1$ oil solubility is enhanced by the C_iE_j, this enhancement is not very large (even at high temperatures) when octane in the major component of the 'co-oil' [22] and T_α remains high. The high value of T_α does not allow the upper critical tie-line to be passed within the experimental window. As a result, $C_m\beta G_1$ never completely partition into the 'co-oil', and a 'chimney' is produced in the three-phase region.

Several authors have examined the role of cosurfactants in water–alkane–$C_m\beta G_1$ microemulsions in terms of the phase diagram represented in Fig. 3. Kahlweit et al. showed that alkanols [18] as well as alkanediols [17,19] can be used to enforce the $\underline{2}$–3–$\overline{2}$ phase sequence in water–

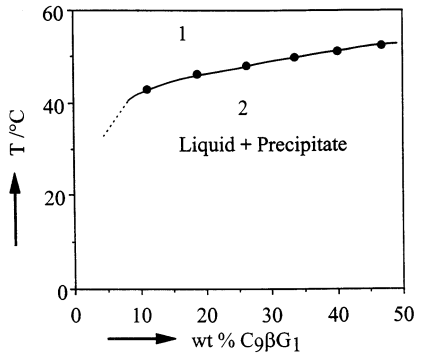

Fig. 4. Binary phase diagram for the $C_3OC_2OC_3$–$C_9\beta G_1$ mixture as a function of temperature and composition.

alkane–C_mG_n mixtures. However, in both cases commercial blends of C_mG_n were used and consequently the phase behavior did not shift substantially with increasing temperature. Others have similarly explored the phase behavior of commercial C_mG_n blends in combination with other classes of cosurfactants [2,15,16]. The results are essentially identical, differing only in the amount of cosurfactant need to traverse the three-phase body. Stubenrauch et al. [20] closely analyzed the water–decane–$C_{10}G_1$ (anomeric mixture)–decanol mixture with respect to phase volumes and densities as a function of increasing δ, tracing the progression through the $\underline{2}$–3–$\overline{2}$ phase sequence. Their results indicate a change in the composition of the microemulsion phase with increasing δ, demonstrated by the abrupt change in density when crossing the three-phase region.

The phase behavior observations from the water–octane–C_6E_2–$C_{10}\beta G_1$ mixture show that C_6E_2 preferentially partitions into octane with increasing temperature. This selective partitioning steadily enriches the microemulsion film with $C_{10}\beta G_1$. The degree of enrichment can be determined quantitatively using a mass balance approach involving the weight fractions of C_6E_2 and $C_{10}\beta G_1$ (C_1 and C_2, respectively) in the microemulsion film. This analysis was first performed by Kunieda et al. [36,37] and has also been applied by Penders and Strey [38] to a water–octane–C_8E_5–octanol mixture and by Stuberauch et al. [21] to a water–cyclohexane–$C_8\beta G_1$–geraniol mixture. Neither of these groups examined the effect of changing temperature on the composition of the interfacial film. If the data shown in Fig. 3 are analyzed following these procedures, at 25°C the microemulsion film is 27% $C_{10}\beta G_1$. At 60°C the surfactant film increases to 58% $C_{10}\beta G_1$. These results clearly reinforce the phase behavior observations discussed above and reiterate the inability of $C_m\beta G_1$ to partition into the oil at high temperature.

3.3. Role of ether oils

From the results shown above and those described in the literature, it is apparent that the value of T_α is extremely high in alkane–C_mG_n mixtures, and producing microemulsions in water–alkane–C_mG_n mixtures without the use of a cosurfactant is nearly impossible. If, however, T_α could be shifted to lower temperatures as a result of employing a class of oils with decreased hydrophobicity, then a cosurfactant would not necessary and the phase behavior of water–oil–$C_m\beta G_1$ microemulsions could be systematically studied and the patterns compared to those observed in the well-known water–alkane–C_iE_j mixtures. Alkyl ethylene glycol ethers ($C_kOC_2OC_k$) are examples of such hydrophilic oils (here k is the number of carbons in the alkyl portions of the molecule). Wormuth and Kaler [39] studied the role of $C_kOC_2OC_k$ in water–$C_kOC_2OC_k$–C_iE_j microemulsions, demonstrating that the increased oil hydrophilicity (relative to alkanes) can eventually move these mixtures past a tricritical point (TCP). It this hydrophilic nature of $C_kOC_2OC_k$-type oils that proves beneficial to forming $C_m\beta G_1$ microemulsions.

3.3.1. $C_9\beta G_1$–$C_3OC_2OC_3$

Fig. 4 shows a partial phase diagram for the binary $C_kOC_2OC_k$–$C_9\beta G_1$ mixture as a function of temperature and surfactant concentration. $C_9\beta G_1$ is completely miscible with $C_3OC_2OC_3$ above 50°C, but below the phase boundary a liquid phase is in equilibrium with a crystalline phase. The phase boundary decreases slightly in temperature as surfactant concentration decreases. Fig. 4 demonstrates that C_mG_1 are considerably more soluble in $C_kOC_2OC_k$ than they

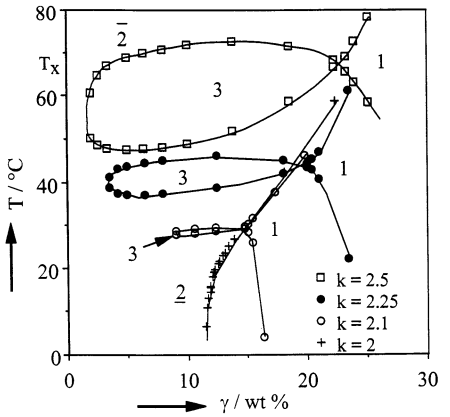

Fig. 5. Vertical sections through the phase prism for mixtures of water–$C_kOC_2OC_k$–$C_8\beta G_1$ as a function of temperature and surfactant concentration (γ) for $k = 2$, 2.1, 2.25, and 2.5. Equal amounts of oil and water are present ($\alpha = 50$).

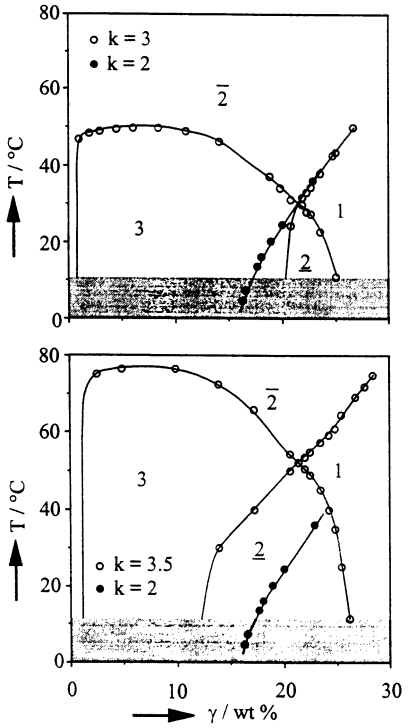

Fig. 6. Vertical sections through the phase prism for mixtures of water–$C_kOC_2OC_k$–$C_{10}\beta G_1$ as a function of temperature and surfactant concentration (γ) for $k = 2$, 3, and 3.5. Equal amounts of oil and water are present ($\alpha = 50$).

are in alkanes. The solubility of other $C_m\beta G_1$ surfactants in $C_kOC_2OC_k$ oils can be inferred from the upper phase boundary of the three-phase region in water–$C_kOC_2OC_k$–$C_m\beta G_1$ mixtures, making further $C_kOC_2OC_k$–$C_m\beta G_1$ phase behavior measurements unnecessary.

3.3.2. Water–$C_kOC_2OC_k$–$C_8\beta G_1$

Fig. 5 shows phase diagrams for mixtures of water–$C_kOC_2OC_k$–$C_8\beta G_1$ as a function of temperature, γ, and increasing alkyl chain carbon number (k) for $\alpha = 50$. When $k = 2$, no three-phase region exists and the mixture is past the tricritical point. As k increases from 2.0 to 2.1, a narrow three-phase body forms. As k further increases to 2.25, the three-phase body widens and moves to higher temperatures. Changing k from 2.1 to 2.5 causes the three-phase body to rise approximately 30°C, and higher values of k move the phase behavior out of the experimental window. The efficiency of the surfactant decreases as k increases.

3.3.3. Water–$C_kOC_2OC_k$–$C_{10}\beta G_1$

Fig. 6 (top) shows a phase diagram for a water–$C_kOC_2OC_k$–$C_{10}\beta G_1$ as a function of temperature, γ, and k for $\alpha = 50$. Again, when $k = 2$, the tricritical point has been passed and only a single-phase region is observed. When $C_{10}\beta G_1$ is used, a large three-phase body covers the experimental window from $\sim$11 to 50°C and the efficiency is $\tilde{\gamma} = 22$, making $C_{10}\beta G_1$ more efficient than $C_9\beta G_1$ for this oil [23]. Below 11°C the mixture is either frozen or contains a precipitate.

Increasing k to 3.5 moves the phase behavior to higher temperatures [Fig. 6 (bottom)]. The three-phase body widens and extends over almost the entire experimental window. The efficiency remains identical to that observed when $k = 3.0$ ($\tilde{\gamma} = 22$). At low surfactant concentration the three-phase region plummets to low temperatures. As is the case when $k = 3.0$, below $\sim$11°C the mixture either contains a precipitate or is completely frozen.

3.3.4. Ether oil discussion

By substituting ether oils for alkanes, $C_m\beta G_1$ oil solubility increases and T_α moves to lower temperatures (Fig. 4). Consequently, water–

$C_kOC_2OC_k$–$C_m\beta G_1$ mixtures are able to produce microemulsions without cosurfactant additives and to undergo the usual $\underline{2}$–3–$\overline{2}$ phase sequence with increasing temperature (Figs. 5 and 6), identical to the behavior observed in water–alkane–C_iE_j mixtures.

As is the case in water–alkane–C_iE_j mixtures [9], the temperature range of the $\underline{2}$–3–$\overline{2}$ phase transition changes with changes in the surfactant structure. While increasing i by 1 (while keeping j and alkane constant) in water–alkane–C_iE_j mixtures moves the phase behavior down only slightly ($\sim$10°C) [9,10], an increase of m by 1 in water–$C_kOC_2OC_k$–$C_m\beta G_1$ mixtures shifts the phase behavior down 30°C (e.g. changing from $C_9\beta G_1$ to $C_{10}\beta G_1$ in a water–$C_3OC_2OC_3$–$C_m\beta G_1$ mixture) [23]. From these results it appears that changes in $C_m\beta G_1$ structure have a larger influence on the phase behavior of water–$C_kOC_2OC_k$–$C_m\beta G_1$ mixtures than does a change in C_iE_j architecture in water–alkane–C_iE_j mixtures. This observation is supported by a similar disparity in the dependence of the value of T_β on changes in $C_m\beta G_1$ and C_iE_j surfactant structure (i.e. in water–$C_m\beta G_1$ mixtures, increasing m by 1 moves T_β down $\sim$80°C [18], while for water–C_iE_j mixtures increasing i by 1 shifts T_β down $\sim$10°C [40]).

The role of $C_m\beta G_1$ structure in changing microemulsion efficiency is not as pronounced as the effects on temperature, but again fits within the framework established for water–alkane–C_iE_j mixtures. $C_m\beta G_1$ efficiency increases for a specified value of k as m increases, indicating increased surfactant amphiphilicity [23]. In water–alkane–C_iE_j mixtures the efficiency increases with increasing amphiphilicity, but usually with the penalty of encroaching liquid crystalline regions, especially with very strong amphiphiles (e.g. $C_{12}E_5$) [9]. For $C_m\beta G_1$ liquid crystalline regions are only observed when $m = 12$ (and presumably for higher values of m), calling into question the relative 'strength' of water–$C_kOC_2OC_k$–$C_m\beta G_1$ microemulsions. Small angle neutron scattering experiments show that $C_m\beta G_1$-based microemulsions are well structured for $m >$ 9 [41], although no liquid crystalline phases are observed within the concentration range studied in the single-phase region. Therefore, although the changes in efficiency with increasing m in water–$C_kOC_2OC_k$–$C_m\beta G_1$ mixtures are not as pronounced as they are for increasing C_iE_j amphiphilicity in water–alkane–C_iE_j mixtures, the general trend towards more strongly structured microemulsions is observed.

The temperature range associated with the $\underline{2}$–3–$\overline{2}$ phase transition in water–oil–nonionic surfactant mixtures also depends on the properties of the oil. For example, for a typical series of water–alkane–C_iE_j mixtures, decreasing the alkane carbon number by 2 (e.g. changing from decane to octane) shifts the three-phase region to lower temperature (by $\sim$10°C), decreases the temperature interval of the three-phase region, and increases the surfactant efficiency [10]. These same trends are observed in mixtures containing water, $C_kOC_2OC_k$, and C_iE_j (e.g. for $C_{12}E_5$ changing k from 3.0 to 2.5 shifts the three-phase region down 5°C) [39]. For water–$C_kOC_2OC_k$–$C_m\beta G_1$ mixtures there are much larger changes in the phase behavior with changing k. For example, in water–$C_kOC_2OC_k$–$C_8\beta G_1$ mixtures (Fig. 5), the three-phase body is very small when $k = 2.1$ (because of the lurking tricritical point [23]) but enlarges substantially and moves up 60°C as k increases from 2.1 to 2.5. Changes of the same magnitude are observed for similar adjustments in the value of k for mixtures containing $C_9\beta G_1$ [23] or $C_{10}\beta G_1$ (Fig. 6). The efficiency of the $C_m\beta G_1$ decreases when k increases, identical to the effects observed in water–oil–C_iE_j mixtures. Therefore, although the qualitative changes in the phase behavior of water–$C_kOC_2OC_k$–$C_m\beta G_1$ mixtures with changes in oil properties are similar to those reported for water–oil–C_iE_j mixtures, the quantitative effects are much larger.

3.4. Surfactant structure effects

Establishing the phase behavior patterns of water–$C_kOC_2OC_k$–$C_m\beta G_1$ mixtures allows for exploration of the effects of other facets of C_mG_n structure on the properties of C_mG_n microemulsions. Two such structural deviations are: (1) the anomeric forms of the sugar headgroup (α-D vs β-D); and (2) additional sugar units in the hydrophilic headgroup (i.e. maltopyranosides,

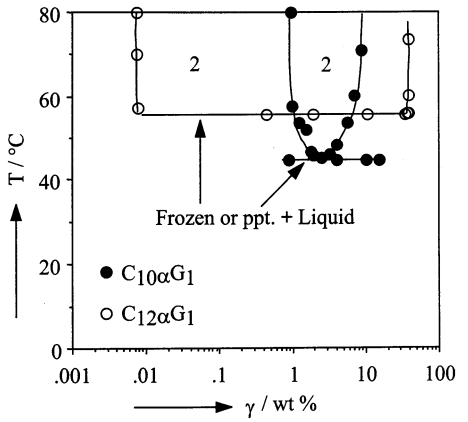

Fig. 7. Binary phase diagrams for water–$C_{10}\alpha G_1$ and water–$C_{12}\alpha G_1$ mixtures as a function of temperature and composition. Note liquid crystalline regions been omitted.

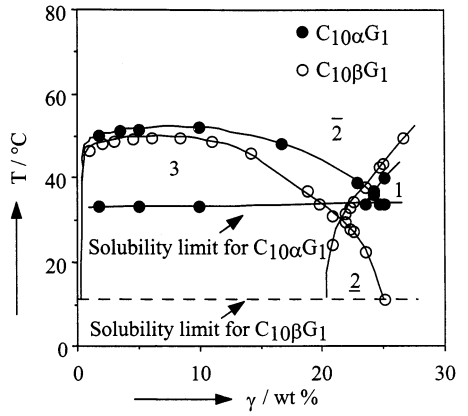

Fig. 8. Vertical section through the phase prism for mixtures of water–$C_3OC_2OC_3$–$C_{10}\alpha G_1$ and water–$C_3OC_2OC_3$–$C_{10}\beta G_1$ as a function of temperature and surfactant concentration (γ). Equal amounts of oil and water are present ($\alpha = 50$).

C_mG_2). These compounds (along with $C_m\beta G_1$) make up the major portion of commercial blends of C_mG_n surfactants, therefore knowledge of phase behavior properties of the individual components leads to better understanding of the blend properties.

3.4.1. Water–$C_m\alpha G_1$

Fig. 7 shows the temperature-composition phase diagrams of binary water–$C_m\alpha G_1$ mixtures for $m = 10$ and 12. When $m = 10$, a narrow miscibility gap extends between $1 < \gamma < 9$ and from 45 to 80°C. Also, there is a Krafft boundary at 44.65°C which extends over the measured concentration range. Interestingly, the upper miscibility gap closes (at a lower critical point) just before contacting the Krafft boundary in the water–$C_{10}\alpha G_1$ mixture. For $m = 12$, the miscibility gap collides with Krafft boundary at 55.65°C. When $m < 10$ (not shown), the $C_m\alpha G_1$ are completely miscible with water but also exhibit Krafft boundaries at 39.5°C for $C_8\alpha G_1$ and at 43.5°C for $C_9\alpha G_1$.

3.4.2. Water–$C_3OC_2OC_3$–$C_{10}G_1$

Fig. 8 shows the temperature-composition phase diagram at $\alpha = 50$ for water–$C_3OC_2OC_3$–$C_{10}G_1$ mixtures containing either $C_{10}\beta G_1$ or $C_{10}\alpha G_1$. As shown in Fig. 6, for $C_{10}\beta G_1$ a large three-phase body covers the experimental window from ~ 11 to 50°C and the efficiency is $\tilde{\gamma} = 22$, while below 11°C the mixture is either frozen or contains a precipitate. Changing from $C_{10}\beta G_1$ to $C_{10}\alpha G_1$ causes the boundary of the precipitate/frozen region to rise up to 34°C, leaving only a small portion of the three-phase body observable (between 34 and 51°C). However, the upper boundary of the three-phase region lies just above that of the three-phase body in the water–$C_3OC_2OC_3$–$C_{10}\beta G_1$ mixture, and the α-D anomer is slightly less efficient (higher $\tilde{\gamma}$) than the β-D anomer.

3.4.3. Water–$C_3OC_2OC_3$–$C_{10}\beta G_1$–$C_{10}G_2$

Fig. 9 shows the temperature-composition phase diagram (at $\alpha = 50$) for water–$C_3OC_2OC_3$–$C_{10}\beta G_1$–$C_{10}G_2$ mixtures as a function of δ. When two surfactants (C and D) are used, γ is defined as $(C + D)/(A + B + C + D)$ (Eq. (2)) and therefore represents the total amount of surfactant. Adding a small amount of $C_{10}G_2$ to the mixture so $\delta = 10$ [Fig. 9 (top)] increases the temperature interval of the three-phase body dramatically and causes the Krafft boundary to disappear, but the efficiency remains unchanged from the $\delta = 0$ case. The three-phase region extends from below 0°C to above 80°C at low values of γ. Increasing δ to 25 [Fig. 9 (bottom)] shifts the phase behavior up in temperature and moves the upper phase boundary above the experimental window. Again, the effi-

ciency of the surfactant mixture does not change substantially. Higher values of δ move the entire three-phase body out of the temperature window.

3.4.4. Surfactant structure discussion

Although typically rare in water–nonionic surfactant mixtures, Krafft boundaries are observed in several mixtures of water and C_mG_1 for both α-D and β-D forms [42]. The Krafft boundary temperature increases with increasing *m* regardless of the anomeric form of C_mG_1, similar to the trend observed in other water–surfactant mixtures with increasing alkyl chain length of the surfactant [43]. However, the additional degree of freedom provided by the anomeric nature of C_mG_1 surfactants allows for a unique comparison between the α-D and β-D forms in aqueous solutions. The most striking difference between water–$C_m\alpha G_1$ and water–$C_m\beta G_1$ mixtures is the ubiquitous presence of Krafft boundaries in water–$C_m\alpha G_1$ mixtures regardless of the value of *m*, while for water–$C_m\beta G_1$ mixtures *m* must be greater than 9 for a Krafft boundary to be observed above 0°C.

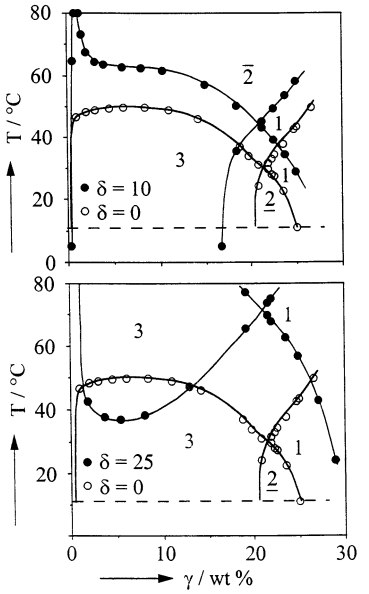

Fig. 9. Vertical sections through the phase prism for of water–$C_3OC_2OC_3$–$C_{10}\beta G_1$–$C_{10}G_2$ mixtures as a function of temperature and surfactant concentration (γ) for $\delta = 0$ (shown on each panel), 10 (top), and 25 (bottom). Equal amounts of oil and water are present ($\alpha = 50$). Dashed line shows solubility limit in water–$C_3OC_2OC_3$–$C_{10}\beta G_1$ mixture.

The discrepancy between the Krafft boundary behavior in water–$C_m\alpha G_1$ mixtures and water–$C_m\beta G_1$ mixtures has been explained in terms of increased crystalline stability of the α-D form. For C_8G_1 compounds [1,24,25,27] the α-D anomer is known to exhibit strong intermolecular hydrogen bonding in both anhydrous [28] and hydrated $C_8\alpha G_1$ crystals [26] (the β-D crystal structure has not been determined). Furthermore, the enthalpy and entropy changes upon melting for $C_8\alpha G_1$ are both more than twice those of $C_8\beta G_1$, as measured by differential scanning calorimetry [27], and at the main solid transition (~ 70°C) $C_8\beta G_1$ loses birefringence while $C_8\alpha G_1$ does not. This experimental evidence supports the conclusion that the increased crystalline stability is most likely as a result of increased hydrogen bonding strength of the α-D form, and this stability moves the Krafft boundary of water–$C_m\alpha G_1$ to higher temperatures than those of the β-D counterparts.

The extension of the Krafft boundary into the Gibbs phase prism at high concentrations of both oil and surfactant further demonstrates the stability of the α-D crystalline form. It is noteworthy that the presence of the solubility boundary does not disrupt the approach to the tricritical point in water–$C_kOC_2OC_k$–$C_8\alpha G_1$ mixtures [29]. This Krafft boundary phenomenon is not usually observed in C_mG_n microemulsions phase behavior, most likely as a result of the use of commercial C_mG_n blends. For commercial blends of C_mG_n surfactants, the Krafft boundary is typically low (< 25°C) [2,5,44–46] as a result of the complex mixture of components, and any corresponding microemulsion behavior is usually studied at or above room temperature (> 25°C) and so is well above any incipient solubility limit in the Gibbs prism.

The hydrophilicity of $C_m\beta G_1$ compounds increases dramatically with the addition of another sugar unit to the head group (C_mG_2 compounds). For example, for water–$C_{10}\beta G_1$ $T_\beta < 0$, while $C_{10}G_2$ is completely miscible with water, indicating T_β rises by more than 80°C when *n* changes from 1 to 2 [18]. By comparison, shifting T_β up by 80°C in water–C_iE_j mixtures requires an increase

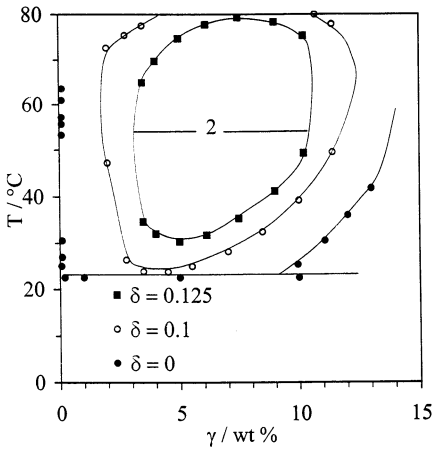

Fig. 10. Temperature-composition phase diagram for water–$C_{10}\beta G_1$–SDeS mixtures with $\delta = 0$, 0.1, and 0.125.

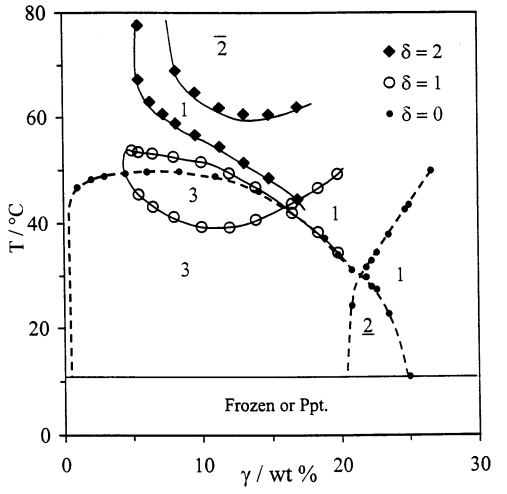

Fig. 11. Vertical sections through the phase prism for mixtures of water–$C_3OC_2OC_3$–$C_{10}\beta G_1$–SDeS at $\alpha = 50$ for $\delta = 0$, 1, and 2. Below ~ 11°C the mixtures are either frozen or contain precipitate for all values of δ.

in *j* of at least 6 [44]. Since the value of T_β changes so drastically with a change from $C_{10}\beta G_1$ to $C_{10}G_2$, it is not surprising that adding $C_{10}G_2$ to water–$C_kOC_2OC_k$–$C_{10}\beta G_1$ mixtures also produces large changes in the phase behavior. As shown in Fig. 9, even small amounts of $C_{10}G_2$ [$\delta = 10$ (top) and 25 (bottom)] added to water–$C_3OC_2OC_3$–$C_{10}\beta G_1$ mixture shift the phase behavior to much higher temperatures, again reflecting the inherent oil insolubility of the sugar headgroup that led to the 'chimney' observed in water–octane–C_iE_j–$C_m\beta G_1$ mixtures. Therefore, systematically producing microemulsions within the experimental temperature range in water–oil–C_mG_2 mixtures requires either a cosurfactant or oils that are even more hydrophilic than the $C_kOC_2OC_k$ compounds.

3.5. Ionic surfactant effects

The amount of surfactant necessary to form microemulsions in water–$C_kOC_2OC_k$–C_mG_n mixtures is quite high (~ 20 wt%) and is of concern in practical applications. However, Kahlweit et al. [30] has shown that adding alkyl sulfates to water–alkane–C_iE_j mixtures can drastically lower $\tilde{\gamma}$. In the next section we apply this approach to water–$C_kOC_2OC_k$–$C_m\beta G_1$ microemulsions, but first consider the role of minute amounts of sodium decyl sulfate (SDeS) on the phase behavior of the water–$C_{10}\beta G_1$ binary mixture.

3.5.1. Water–$C_{10}\beta G_1$–sodium decyl sulfate (SDeS)

Fig. 10 shows the temperature-composition phase diagrams for water–$C_{10}\beta G_1$–SDeS mixtures for $\delta = 0$, 0.1, and 0.125. When $\delta = 0$, the miscibility gap extends between $0.01 < \gamma < 13$, and collides with the Krafft boundary at ~ 22.5°C, thereby obscuring the location of the lower critical point (T_β). Increasing δ to 0.1 (molar ratio of 0.0012) shifts T_β above the Krafft boundary and the entire miscibility gap shrinks. When $\delta = 0.125$ (molar ratio of 0.0015), the miscibility gap continues to shrink in both temperature and composition range. A further increase in δ to 0.15 causes the miscibility gap to become vanishingly small (not shown), and when $\delta = 0.2$ it disappears altogether and the mixture forms a single isotropic phase over the measured concentration and temperature range.

3.5.2. Water–$C_3OC_2OC_3$–$C_{10}\beta G_1$–SDeS

Fig. 11 shows temperature-composition phase diagrams at $\alpha = 50$ for water–$C_3OC_2OC_3$–$C_{10}\beta G_1$–SDeS mixtures with $\delta = 0$, 1, and 2. When $\delta = 0$, $\tilde{\gamma} = 21$ and the three-phase region

extends to very low temperatures (~ 10°C). Increasing δ to 1 dramatically increases the efficiency ($\tilde{\gamma} = 16$) and shifts the three-phase region to higher temperatures. Also, the three-phase body distorts and tilts to higher temperatures as γ decreases. Further increasing δ to 2 again vastly improves the efficiency ($\tilde{\gamma} = 5.5$), and the three-phase body disappears completely. Further increases in δ (not shown) move the single-phase region above the experimental window and slightly decrease the efficiency of the surfactant mixture. Below ~11°C the solution is either frozen or contains a precipitate for all values of δ.

3.5.3. Ionic surfactant discussion

It is remarkable that tiny amounts of SDeS added to water–$C_{10}\beta G_1$ mixtures produce such large changes in the phase behavior. For instance, even at a molar ratio of 0.0012 ($\delta = 0.1$), adding SDeS to the water–$C_{10}\beta G_1$ binary mixture causes the miscibility gap to rise in temperature and pull away from the Krafft boundary (Fig. 10). A further increase in molar ratio to 0.0025 ($\delta = 2$) causes the miscibility gap to vanish completely. This pattern of phase behavior is qualitatively similar to that observed for several water–C_iE_j–ionic surfactant mixtures [47–50], but smaller amounts of SDeS are needed to produce larger changes in the phase behavior of the water–$C_{10}\beta G_1$ mixture. This phenomenon has been further confirmed for mixtures of water–alkyl sulfates and commercial C_mG_n blends [44].

Adding ionic surfactants to water–C_iE_j mixtures is known to shift T_β to higher temperature and shrink the upper miscibility gap as a result of the electrostatic intermicellar repulsion caused by the partitioning of the ionic surfactant into the nonionic micelle [44,47–49,51–53]. The intensity of the electrostatic repulsion has been tracked experimentally for several water–C_iE_j–ionic surfactant mixtures [51,53,54]. Balzer [44] determined that C_mG_n micelles show a greater affinity for incorporation of alkyl sulfates than do C_iE_j micelles and therefore exhibit a stronger electrostatic repulsion for smaller ionic surfactant concentration. These conclusions are further supported by the disappearance of the upper miscibility gap in water–$C_{10}\beta G_1$–SDeS mixtures (Fig. 10) with increasing SDeS concentration.

Experimentally, the major effects caused by the addition of alkyl sulfates to water–$C_kOC_2OC_k$–$C_m\beta G_1$ mixtures are increased efficiency of the surfactant mixture, shifting of the phase behavior to higher temperatures, and the shrinkage and eventual disappearance of the three-phase region with increasing ionic surfactant concentration [31]. These phase behavior trends are similar to those observed in water–alkane–C_iE_j–alkyl sulfate mixtures [30]. The patterns of phase behavior in water–alkane–C_iE_j–alkyl sulfate mixtures result from a combination of electrostatic stabilization of oil-swollen micelles along the water-rich portion of the phase prism [55,56] and coinciding minor role of the ionic surfactant along the oil-rich side of the phase prism. These unequal effects distort and skew the three-phase region to higher temperatures. This explanation for the patterns of phase behavior observed in water–alkane–C_iE_j–alkyl sulfate mixtures can be directly applied to water–$C_kOC_2OC_k$–$C_{10}\beta G_1$–SDeS mixtures and is supported by the data in Fig. 11.

The increased surfactant efficiency observed in water–$C_kOC_2OC_k$–$C_m\beta G_1$–alkyl sulfate mixtures can be explained by the electrostatic interactions introduced with the addition of ionic surfactant to the surfactant monolayer. In microemulsions, the surfactant monolayers are known to be 'floppy' and undergo sterically stabilizing undulations [57–59], which leads to a rather inefficient use of interfacial area. Adding ionic surfactant suppresses these undulations thereby producing a more rigid monolayer [60,61]. Increasing the rigidity of the surfactant monolayer has two main effects: (1) the interfacial area lost to undulations is regained; and (2) the monolayer spacing increases as a result of electrostatic interactions between monolayers. The combination of these two effects leads to a more efficient use of the interfacial area and consequently leads to more efficient microemulsions. Therefore, it is perhaps not surprising that adding alkyl sulfates to water–$C_kOC_2OC_k$–$C_{10}\beta G_1$ mixtures enhances surfactant efficiency. The earliest report of this phenomena is as a result of Shinoda and Kunieda [62].

4. Conclusions

This review of alkyl polyglucoside microemulsion phase behavior summarizes several important aspects of producing microemulsions with C_mG_n surfactants. Unusually low solubility in alkanes necessitates the use of a cosurfactant to produce microemulsions with water, alkane, and C_mG_n. However, even with a cosurfactant such as C_iE_j, the $\underline{2}$–3–$\overline{2}$ phase sequence is not fully observed in water–octane–C_iE_j–$C_m\beta G_1$ mixtures; instead a temperature-independent 'chimney' is observed at low surfactant concentrations. Changing to more hydrophilic $C_kOC_2OC_k$ oils increases C_mG_n oil solubility (lowers T_α) and water–$C_kOC_2OC_k$–$C_m\beta G_1$ mixtures exhibit patterns of phase behavior identical to those observed in water–alkane –C_iE_j mixtures. Changing from the β-D to the more stable α-D anomeric form causes the solubility boundary to move to much higher temperature in water–C_mG_1 and water–$C_kOC_2OC_k$–C_mG_1 mixtures. Increasing C_mG_n hydrophilicity by adding a sugar unit to the headgroup (C_mG_2) shifts the phase behavior to much higher temperatures, again reflecting the low oil solubility of the sugar moiety. Finally, the efficiency of water–$C_kOC_2OC_k$–$C_m\beta G_1$ microemulsions increases dramatically with the addition of small amounts of ionic surfactant additive as a result of electrostatic stabilization of the microemulsion surfactant monolayers.

Acknowledgements

This research was funded by ICI Surfactants.

References

[1] F. Nilsson, INFORM 7 (1996) 490–497.
[2] W. von Rybinski, Curr. Opin. Colloid Interface Sci. 1 (1996) 587–597.
[3] K. Hill, W. von Rybinski, G. Stoll, Alkyl Polyglucosides: Technology, Properties, and Applications, VCH, New York, 1997.
[4] R.A. Aleksejczyk, in: B.N. Devisetty, D.G. Chasin, P.D. Berger (Eds.), Pesticide Formulations and Application Systems: 12th Volume, vol. 12, ASTM, Philadelphia, 1993, pp. 22–32.
[5] D. Balzer, Tenside Surf. Det. 28 (1991) 419–426.
[6] R.M. Hill, S.O. Dieker, Presented at 78th AOCS Meeting, New Orleans, 1987.
[7] K. Hill, in: K. Hill, W. von Rybinski, G. Stoll (Eds.), Alkyl Polyglucosides: Technology, Properties and Applications, VCH, New York, 1997, pp. 1–7.
[8] R. Leung, M.J. Hou, D.O. Shah, in: D.T. Wasan, M.E. Ginn, D.O. Shah (Eds.), Surfactants in Chemical/Process Engineering, vol. 28, Marcel Dekker, New York, 1988, pp. 315–367.
[9] M. Kahlweit, R. Strey, P. Firman, D. Haase, J. Jen, R. Schomäcker, Langmuir 4 (1988) 499–511.
[10] M. Kahlweit, R. Strey, P. Firman, J. Phys. Chem. 90 (1986) 671–677.
[11] K.-V. Schubert, E.W. Kaler, Ber. Bunsenges. Phys. Chem. 100 (1996) 190–205.
[12] M. Kahlweit, R. Strey, P. Firman, D. Haase, Langmuir 1 (1985) 281–288.
[13] M. Kahlweit, R. Strey, Angew. Chem. Int. Ed. Engl. 24 (1985) 654–668.
[14] M. Kahlweit, Tenside Surf. Det. 30 (1993) 83–89.
[15] K. Fukuda, O. Söderman, B. Lindman, K. Shinoda, Langmuir 9 (1993) 2921–2925.
[16] T. Förster, B. Guckenbiehl, H. Hensen, W. von Rybinski, Prog. Coll. Polym. Sci. 101 (1996) 105–112.
[17] M. Kahlweit, G. Busse, B. Faulhaber, Langmuir 12 (1996) 861–862.
[18] M. Kahlweit, G. Busse, B. Faulhaber, Langmuir 11 (1995) 3382–3387.
[19] M. Kahlweit, G. Busse, B. Faulhaber, Langmuir 13 (1997) 5249–5251.
[20] C. Stubenrauch, E.-M. Kutschmann, B. Paeplow, G.H. Findenegg, Tenside Surf. Det. 33 (1996) 237–241.
[21] C. Stubenrauch, B. Paeplow, G.H. Findenegg, Langmuir 13 (1997) 3652–3658.
[22] L.D. Ryan, K.-V. Schubert, E.W. Kaler, Langmuir 13 (1997) 1510–1518.
[23] L.D. Ryan, E.W. Kaler, Langmuir 13 (1997) 5222–5228.
[24] G.M. Brown, P. Dubreuil, F.M. Ichhaporia, J.E. Desnoyers, Can. J. Chem. 48 (1970) 2525–2531.
[25] D.L. Dorset, J.P. Rosenbusch, Chem. Phys. Lipids 29 (1981) 299–307.
[26] G.A. Jeffrey, Y. Yeon, J. Abola, Carbohydr. Res. 169 (1987) 1–11.
[27] A.J.J. Straathof, H. van Bekkum, A.P.G. Kieboom, Starch 40 (1988) 438–440.
[28] H. van Koningsveld, J.C. Jansen, A.J.J. Straathof, Acta Crystallogr. Sect. C 44 (1988) 1054–1057.
[29] L.D. Ryan, E.W. Kaler, J. Colloid Interface Sci. 210 (1999) 251–260.
[30] M. Kahlweit, B. Faulhaber, G. Busse, Langmuir 10 (1994) 2528–2532.
[31] L.D. Ryan, E.W. Kaler, J. Phys. Chem. B 102 (1999) 7549–7556.
[32] M. Kahlweit, E. Lessner, R. Strey, J. Phys. Chem. 88 (1984) 1937–1944.

[33] M. Kahlweit, R. Strey, G. Busse, Phys. Rev. E 47 (1993) 4197–4209.
[34] K.-V. Schubert, R. Strey, J. Chem. Phys. 95 (1991) 8532–8545.
[35] K. Shinoda, T. Yamaguchi, R. Hori, Bull. Chem. Soc. Jpn. 34 (1961) 237–241.
[36] H. Kunieda, K. Shinoda, J. Colloid Interface Sci. 107 (1985) 107–121.
[37] H. Kunieda, A. Nakano, M. Akimaru, J. Colloid Interface Sci. 170 (1995) 78–84.
[38] M.H.G.M. Penders, R. Strey, J. Phys. Chem. 99 (1995) 10313–10318.
[39] K.R. Wormuth, E.W. Kaler, J. Phys. Chem. 93 (1989) 4855–4861.
[40] K.-V. Schubert, R. Strey, M. Kahlweit, J. Colloid Interface Sci. 141 (1991) 21–29.
[41] L.D. Ryan, E.W. Kaler, Langmuir 15 (1999) 92–101.
[42] F. Nilsson, O. Söderman, I. Johansson, Langmuir 13 (1997) 3349–3354.
[43] R.G. Laughlin, The Aqueous Phase Behavior of Surfactants, Academic Press, New York, 1994.
[44] D. Balzer, Langmuir 9 (1993) 3375–3384.
[45] D. Nickel, T. Förster, W. von Rybinski, in: K. Hill, W. von Rybinski, G. Stoll (Eds.), Alkyl Polyglucosides: Technology, Properties and Applications, VCH, New York, 1997, pp. 39–69.
[46] G. Platz, C. Thunig, J. Pölicke, W. Kirchoff, D. Nickel, Colloids Surf. A 88 (1994) 113–122.
[47] C.B. Douglas, E.W. Kaler, Langmuir 7 (1991) 1097–1102.
[48] L. Marszall, Langmuir 4 (1988) 90–93.
[49] G. Komaromy-Hiller, N. Calkins, R. von Wandruszka, Langmuir 12 (1996) 916–920.
[50] P. Firman, D. Haase, J. Jen, M. Kahlweit, R. Strey, Langmuir 1 (1985) 718–724.
[51] C.B. Douglas, E.W. Kaler, Langmuir 10 (1994) 1075–1083.
[52] L. Marszall, Langmuir 6 (1990) 347–350.
[53] P.-G. Nilsson, B. Lindman, J. Phys. Chem. 88 (1984) 5391–5397.
[54] C.B. Douglas, E.W. Kaler, J Chem. Soc. Faraday Trans. 90 (1994) 471–477.
[55] D.B. Siano, P. Myer, J. Bock, J. Colloid Interface Sci. 117 (1987) 534–543.
[56] D.B. Siano, P. Myer, J. Bock, J. Colloid Interface Sci. 117 (1987) 544–549.
[57] R. Strey, J. Winkler, L. Magid, J. Phys. Chem. 95 (1991) 7502–7507.
[58] D. Morse, Curr. Opin. Colloid Interface Sci. 2 (1997) 365–372.
[59] P.G. De Gennes, C. Taupin, J. Phys. Chem. 86 (1982) 2294–2304.
[60] K. Fukuda, U. Olsson, Langmuir 10 (1994) 3222–3229.
[61] V. Rajagopalan, H. Bagger-Jörgensen, K. Fukuda, U. Olsson, B. Jönsson, Langmuir 12 (1996) 2939–2946.
[62] K. Shinoda, H. Kunieda, J. Colloid Interface Sci. 42 (1973) 381.